Energy 313 (2024) 133743

Contents lists available at ScienceDirect

Energy

journal homepage: www.elsevier.com/locate/energy

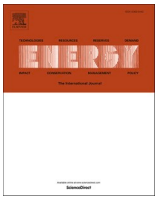

Energy, exergy and exergo-economic analyses of supercritical CO_2 cycles for the exploitation of a geothermal resource in the Italian water dominant Amiata site

N. Di Michele, L. Talluri, P. Ungar, D. Fiaschi *

Department of Industrial Engineering, University of Florence, Florence, Via S. Marta 3, 50139, Italy

ARTICLE INFO

Keywords:
Geothermal energy
Binary cycle
sCO_2
Exergo economic
Electricity production cost

ABSTRACT

Alternative powerplant layouts to commonly applied flash technology is investigated for the water dominant geothermal location of Amiata Mountain, Italy. The proposed solution avoids flashing the brine stream by a borehole pump capable of maintaining pressurized conditions, thus reducing the amount of non-condensable gases released when reaching the ground level. Therefore, the need of a gas treatment section is completely avoided. The heat recovered from the hot brine at ground level is transferred to different supercritical CO_2 cycle configurations, equipped with high efficiency Printed Circuit Heat Exchangers (PCHE). The optimal 45.5 % calculated exergy efficiency was achieved for the recuperative cycle with intercooling and reheat, which however didn't show the optimal electricity costs (8.092 c€/kWh) because of the more complex heat exchangers network. The lowest cost of electricity (7.4 c€/kWh) was found for the recuperative cycle configuration. These costs are in line with the current levels of geothermal binary cycles, but almost doubled compared to the current single flash + ORC solution, due to a 40–50 % reduction of power output with sCO_2 cycles. On the other hand, sCO_2 binary cycles could guarantee an almost zero environmental impact, which is the main reason for social concerns related to the current flash powerplants.

1. Introduction

The energy demand has increased exponentially in recent years due to the strong increase in economic development and population growth. This led to an increased concern on sustainability issues and environmental deterioration [1]. The exploitation of renewable energy technologies has therefore bloomed, allowing an increase in the efficiency of the conversion systems. Among renewables, geothermal energy has the advantage of having the highest resource availability, not depending on the weather conditions. Geothermal energy systems exploit the heat content of the earth's interior, as the earth is slowly cooling down. The total global output of the Earth's heat flow is over 4×10^{13} W [2], which is four times higher than the actual energy consumption; however, only a small part of this heat flux can be exploited. Geothermal power plants can be categorized in shallow geothermal and deep geothermal. The first exploits low temperature heat sources at the surface, with a maximum of well drilling in the range of 250 m and are suitable for low temperature heat generation. On the other hand, deep geothermal is considered when wells are drilled deep, from 1 to 5 km within the Earth, or even deeper with the newest drilling technologies. Deep geothermal allows reaching higher temperature, which enables the conversion of the geothermal heat in electricity. Another way to categorize geothermal power plant is to classify it on the enthalpy content of the flow: low, medium or high enthalpy. Medium and high enthalpy resources are the most common exploited and have almost reached its maximum potential, while low or moderate enthalpy fields are still yet to be fully utilized. Typical power plant for the exploitation of medium high temperature fields are single, double and triple flash power plants (for a water dominant reservoirs) and direct steam power plants (for vapor dominant reservoirs). These power plants have several advantages such as relatively high conversion efficiencies, several years of operation which led to a solid know-how, well-known safety measures which are not critical thanks to low pressure and temperatures involved, and economic feasibility. On the other hand, they present a significant disadvantage when considering the environmental sustainability; indeed, a relevant documented issue is the release of non-condensable gases NCGs (mainly CO_2 plus several kind of contaminants) to the environment [3,4]. The current solution to reduce the environmental impact of geothermal power plant is the utilization of AMIS technology in Italy, developed by ENEL GP [5]. This allows to

* Corresponding author.
E-mail address: daniele.fiaschi@unifi.it (D. Fiaschi).

https://doi.org/10.1016/j.energy.2024.133743
Received 30 November 2023; Received in revised form 27 June 2024; Accepted 23 August 2024
Available online 12 November 2024
0360-5442/© 2024 The Author(s). Published by Elsevier Ltd. This is an open access article under the CC BY license (http://creativecommons.org/licenses/by/4.0/).

Nomenclature

Symbols

c_{j_k}, c_{i_k}	Flux costs, [€/kJ]
$cost_{fuel_{kJ}}$	Geothermal fluid specific exergy cost, [€/kJ]
$cost_{Wt_{kJ}}$	Turbine power specific cost, [€/kJ]
$cost_{kWh_{el}}$	Produced KWh cost, $\left[\frac{c€}{kWh}\right]$
$\dot{C}_P$	Output product cost, [€/s]
$\dot{C}_F$	Fuel cost, [€/s]
ex	Specific exergy, [kJ/kg]
h	Enthalpy, [kJ/kg]
P	Pressure, [Pa, bar]
Q	Thermal power, [kW]
s	Entropy, [kJ/kg-K]
T	Temperature [K, °C]
$\dot{Z}$	Capital Investment
W	Power, [kW]
$\dot{m}$	Mass flow rate, [kg/s]

Greek symbols

η	First law efficiency, [−]
η_{II}	Second law efficiency, [−]
ρ	Density, [kg m^{-2}]
Δ	Difference

Subscripts

0	Reference state
1, 2, 3, …	Cycle reference points
Approach	Geofluid – CO_2 cycles Temperature difference
Geo	Geothermal fluid
in/out	Inlet/Outlet

Acronyms

CEPCI –	Chemical Engineering Plant Cost Index
PEC –	Purchased equipment costs

reduce the Hg and SO_2 content from the NCGs stream, reducing the environmental impact of the power plants. Several studies have been developed on the environmental sustainability of geothermal energy conversion systems though the application of life cycle assessment [6,7]. In Ref. [8] a 20 MW single flash power plant is evaluated and compared with similar size power plants operating with wind and solar. It was found that the geothermal power plant, which includes the AMIS technology, performs well against other renewables, and has only a slightly higher environmental footprint, due to larger values of the global warming category (Recipe 2016 Midpoint). In Ref. [9] enhanced geothermal systems (EGS) were considered, estimating several design scenarios and compared to other renewable energies environmental impacts. The results indicated that EGS power plant environmental footprint is in the same range of other renewables and it was confirmed that the highest contribution to the environmental impact comes from the drilling of the wells, and in particular by the diesel burned in the drilling process. In Ref. [10], the environmental impact of a combined heat and power double flash geothermal power plant was estimated. In their study, it was again confirmed that the drilling process is the main responsible for most of the impact category results, however, it was also found that the global warming and acidification category are significantly affected by the operation phase. Indeed, during the operational lifetime of the power plant, continuous emissions of CO_2 and H_2S provide a significant environmental impact. In Ref. [11] the definition of harmonized LCA guidelines for the comparison of geothermal power plant have been drought. Particularly, the aim of their study was to increase the comparability of the results of LCA studies on geothermal system, by proposing a consistent methodology with several indications of the critical aspects of the analysis.

From the above mentioned studies, it seems that only the use of binary cycles (like ORCs, Kalina or trans-critical and supercritical CO_2) coupled to the complete reinjection of NCGs could give a valuable answer to the improvement of sustainability of geothermal power plants, particularly in the operational phase [12]. ORC and Kalina cycles work with novel and environmentally friendly fluids (low GWP), which are suitable for the exploitation of low temperature resources. Several studies on the coupling of ORC or Kalina cycles with low temperature or medium-high temperature geothermal resources have been performed [13–17]. These studies involved the optimal selection of the working fluid [18], including zeotropic mixtures [19], the optimal configuration of the power plant [20,21], as well as thermo-economic analysis [22]. In Ref. [23] an energy and exergy analysis are carried out for a dual fluid ORC. Isobutane and Isopentane were selected as working fluids, allowing a production of almost 3.5 MW of electricity, almost equally shared between the high temperature isopentane cycle and the low temperature isobutane cycle. The most critical components for this power cycle configuration were found to be the low and high pressure vapor generators, due to the not optimal match of the composite heat transfer curves. An interesting study on the profitability of geothermal electricity production from several ORC configurations have been carried out in Ref. [24]. In their study, an optimization of cycle configurations, working fluid selection and thermodynamic conditions was carried out in order to investigate the most performing configuration, based on levelized cost of electricity, return of investment and payback period. They performed the analysis taking into account for the economic calculation, the corporate tax rates and the average electricity prices of 20 countries and found that the country with the highest return of investment was the one with highest electricity price. A focus on the design and optimization of the evaporator for ORCs for low temperature geothermal application has been developed in Ref. [25]. In their study a Pareto front solution has been found in order to assess the proper compromise between costs and pressure drop in the heat exchanger; finally evaluating the performance of the ORC.

While several studies on ORC and Kalina cycle for geothermal applications have been developed, on the other hand, few studies on the coupling of supercritical CO_2 cycles with geothermal energy resources have been developed. In Ref. [26] a trans critical power cycle for low temperature geothermal power plants has been investigated, with a particular focus of the influence of the recuperator performance in both design and off-design operation. It was found that the recuperator allows an improvement in the off-design performance of the system, particularly enhancing the performance of the CO_2 pump. In Ref. [27] an innovative supercritical CO_2 cycle configuration was evaluated, and its performance compared to a ORC working with R245fa or R1233zd(E). The cycle configuration exploits the thermosiphon concept, therefore utilizing the CO_2 both as heat medium in the reservoir and as the working fluid in the power cycle. The results obtained indicated that the ORC cycle with R245fa as working fluid allowed the highest power production for one year of operation (8 % more than the sCO_2 thermosiphon cycle). In Ref. [28] a low temperature geothermal case study, the Sidirokastron field in Greece is studied in order to couple a supercritical CO_2 power plant. Particularly, the maximum temperature achieved by the geothermal fluid is 75 °C, a very low value which hinders thermodynamic efficiency. In these conditions, the sCO_2 cycle achieved a maximum thermal efficiency slightly above 6 %. Another interesting study by Ref. [29] deals with the thermodynamic analysis of a low temperature geothermal power plant utilizing a mixture of SF_6 and CO_2 as working fluid. The maximum achieved efficiency of the binary

geothermal cycles was found to be 15 % with a 20 % SF_6-80 % CO_2 composition, with a resource temperature of 160 °C. The results therefore indicated that the utilization of zeotropic CO_2 mixtures could allow to increase the thermal efficiency of the sCO_2 power plants for geothermal applications.

While few studied have been focused on the coupling of supercritical CO_2 cycles with low temperature geothermal application, on the other hand several studies are found in literature when dealing with high temperature applications, like solar power generation [30], coal fired power plants [31] or waste heat recovery [32,33]. This is due to the very good behaviour of the CO_2 for high temperature applications, nonetheless, it seems that further studies are needed to provide a clear assessment on the application of CO_2 cycle to low temperature resource. However, recently a few Authors proposed the use of super and trans critical CO_2 cycles to exploit low to medium temperature geothermal resources in binary configurations. For example [34], analysed the thermodynamic performance and optimization of transcritical power cycles (TPCs) using CO_2-based binary zeotropic mixtures for the conversion of low grade geothermal water at 100–150 °C [35]. carried out a comparative thermoeconomic analysis of geothermal energy recovery via super/transcritical CO_2 and subcritical organic Rankine cycles in the 5–7 MWel size range for a 170 °C resource, achieving LCOE in the range of 0.12–0.16 $/kWh and showing that the transcritical CO_2 configuration has the lowest payback period. On 2023 [36,37], proposed a techno-economic assessment of s CO_2 Brayton cycles for low-grade geothermal reservoirs (150 °C), achieving the best thermo-economic performance with the 930-kW intercooled recuperated Brayton cycle. In their analysis, they adopted Printed Circuit Heat Exchangers (PCHEs) with straight semi-circular channels because of their suitability and wide use in CO_2-based systems due to their compactness and structural stiffness, which helps to withstand the high pressures of the sCO_2. This solution has been also adopted in the present proposal.

Indeed, the selection of CO_2 as working fluid is due to its main characteristics, such as non-toxic, non-flammable, not suffering any thermal degradation at high temperature (unlike ORCs fluids) and optimal environmental traits, with a null ODP and a GWP = 1. Furthermore, in the supercritical region, the high density of the CO_2 allows a smaller and more compact design of the components, which could allow a “miniaturize” design of geothermal power plants. Various benefits and versatility of sCO2 in heat transfer and cooling purposes are addressed in works by Manda et al. Group. In Ref. [38], the Authors compared the heat transfer characteristics of flow of sCO_2 and water inside a square microchannel, achieving half value of pressure drop for sCO_2. In Ref. [62], a comparative analysis of ammonia and sCO_2 for Microchannel Cooling was carried out. They concluded that, at the fixed same mass flux, ammonia gave higher average heat transfer coefficient but at the same pressure drop, sCO_2 resulted in higher heat transfer coefficient at certain surface temperatures. The Coefficient Of Performance (COP) was ultra-high for sCO_2 (600,000 level) and it was significantly higher than that for ammonia. In their very recent work [39], investigated the effects of cross-sectional shape on flow and heat transfer of laminar sCO_2 flow inside horizontal microchannels, concluding that the microchannel with triangular cross-section has the highest heat transfer rate, highest mass flow rate, and lowest pressure drop. The excellent performance of a star-shaped cross-sectional Microchannel with sCO_2 was discussed in Ref. [64].

Finally, for variable temperature heat source, supercritical CO_2 allow a better match of the profiles, guaranteeing a higher efficiency of the heat transfer and thus reducing the exergy losses in the heat exchanger. The present proposal is aimed at investigating the possible adoption of binary sCO_2 cycles in different possible layouts coupled to the high temperature water dominant geothermal resource of the Italian Amiata field, currently exploited into a 20 MW flash powerplant. Moreover, in the present proposal, the adoption of a borehole pump within the well is investigated, in order to avoid the flash of the resource. The introduction of a borehole pump implies additional uncertainties related to the resistance of the pump itself into the corrosive environment of the hot geothermal brine. The lifespan of the borehole pump is very difficult to predict as operational time ranging from multiple months (potentially years) [40,41] to few days [41,42] are reported in literature. The lifespan depending mainly on the pump design [41] and on the chemical composition and temperature of the brine [42,43]. According to the classification proposed by Ellis and Conover [44], the brine in the Mt. Amiata region should not be very corrosive if compared with other geothermal reservoir given the fact that is has a relatively neutral pH [45] and a small concentration of corrosive species, such as H_2S, being the NCGs emission composed mainly of CO_2 [45]. This means that installing a borehole pump in these conditions should easier than in other cases, making it an interesting solution to be tested. For comparison, a pump installed in a well of the EGS reservoir in Soultz, which has a much more challenging condition for material corrosion (pH = 4.7, T = 200 °C [46]) has lasted 6 months without failing before being removed for inspection [41]. Nevertheless, a complete analysis of the expected lifetime of such an equipment is beyond the scope of this research. The results in terms of thermodynamic performance and thermo-economic costs of electricity production of the sCO_2 cycles, may be relevant in assessing the feasibility of a possible closed – loop clean alternative to flash powerplants in fields, like the Amiata one, where the pollutant emissions associated to the current use of the resource are raising environmental and social concerns. This work could be seen as an follow up of the work of Ruiz-Casanova and his colleagues [36,37]. The novelty introduced in this analysis is the comparison with an existing geothermal power plant by means of an extensive exergo-economic analysis to better asses the potential of this solution. Moreover, more complex CO_2 cycles have been analysed to identify the most promising solution and a borehole pump installation has been considered to avoid flashing and reducing scaling in the production well.

1.1. A case study for a sustainable geothermal energy power plant (Mount Amiata, Italy)

The properties of the geothermal resource are variable depending on the location in terms of pressure, temperature, state of the fluid, and amount and composition of NCGs as well as of dissolved mineral salts. The nature of contaminants released by GECS usually includes H_2S, NH_3, CH_4, and in some cases Hg [47–49]. Each potential location deserves careful study, possibly leading to different issues when selecting the best available technology.

The area of Mount Amiata, Italy, represents a significant challenging application. This region of Southern Tuscany is historically one of the reference sites for the development of geothermal conversion systems; currently, about 80 MW of geothermal electricity are installed there. The Amiata reservoir is water-dominant type [50]; the current conversion technology applies single or double-flash power plant layouts, in one case also combined to an ORC to recover the energy content in brines. The composition of the geofluid includes relevant amounts of NCGs (CO_2, H_2S, NH_3, CH_4), mercury sulphide, HgS and dissolved salts (mainly stibnite and silica salts). The reservoir is located at 3000–3500 m depth, thereby determining supercritical pressure conditions (p > 250 bar); however, the fluid is not in critical conditions, since the reservoir temperature is in the 300–350 °C range. Consequently, flashing in the well takes place at a depth between 600 and 1500 m, with two-phase flow in the upper section. In the current technology, a throttling valve/separator assembly is located at the wellhead [51,52]. Despite the attractiveness of the region in terms of energy generation potential, local opposition is present in the area against further development of geothermal energy. The main concerns of the opponents are long-term sanitary effects (mainly traceable to Hg and H_2S emissions, even after the introduction of catalytic gas treatment [5]), as well as the water balance and the greenhouse gas emissions. Within this context, even if the resource can be classified as high-enthalpy and therefore traditionally converted using flash power plant solutions, it makes sense

to explore different possible options, investigating the potential to mitigate these specific issues.

1.2. Reference case

As a specific reference case, the available data from the Bagnore 3 power plant were considered. A flow rate of 122 kg/s is assumed to be available at an enthalpy level of 1200 kJ/kg, corresponding to about 275 °C at 250 bar, which are the estimated reservoir conditions for the deep reservoir in the Mt. Amiata region at a depth z > 3000 m. The CO_2 content of the brine is evaluated at 2 % mass fraction [53]. The current power plant applies a wellhead separator set at 20 bar, determining a saturated steam flow rate of 36 kg/s (with 7 % CO_2 content), while a hot brine (enriched with salts causing considerable scaling problems) of about 86 kg/s is directed to reinjection. The power plant is a single-flash unit equipped with an ORC recovery section on a secondary (low-pressure) flash of the brine, providing a total power output of about 23 MWe (actually, at present 3 MWe less because a smaller ORC unit is installed, with incomplete heat recovery from the reinjection brine). The separator setting determines the flash conditions inside the well, which take place at a depth of about 600 m. The considerable amount of CO_2 in the flash steam is accompanied by minor contaminants (H_2S, Hg and NH_3 with minor traces of CH_4); while the steam is condensed in the steam cycle, the NCGs are discharged to the atmosphere; however, before the final release, the emissions treatment is applied, with extensive capture of H_2S, Hg and NH_3. The following emissions levels were calculated: e_{CO2} = 396 g/kWh; e_{H2S} = 1.21 g/kWh; e_{Hg} = 1.3 g/kWh; these figures correspond to measurements taken by the pollution control authority. It should be underlined that the CO_2 emissions are of natural origin; however, they are of similar level to those obtained by the most advanced fossil fuel power plants and could be avoided if the resource was not extracted from the reservoir.

For the above reasons, a number of improved solutions were developed, leading finally to identifying guideline the complete reinjection of NCGs in the reservoir as a possible best practice to exploit this geothermal resource [53].

To summarize, the literature review and the analysis of the presented case study has indicated a significant gap in the study of supercritical CO_2 cycle for the exploitation of geothermal resources.

Specifically, in the present study a relatively simple solution is proposed, inspired by the guideline of completely avoiding the practice of flashing the geothermal stream by the means of a borehole pump located

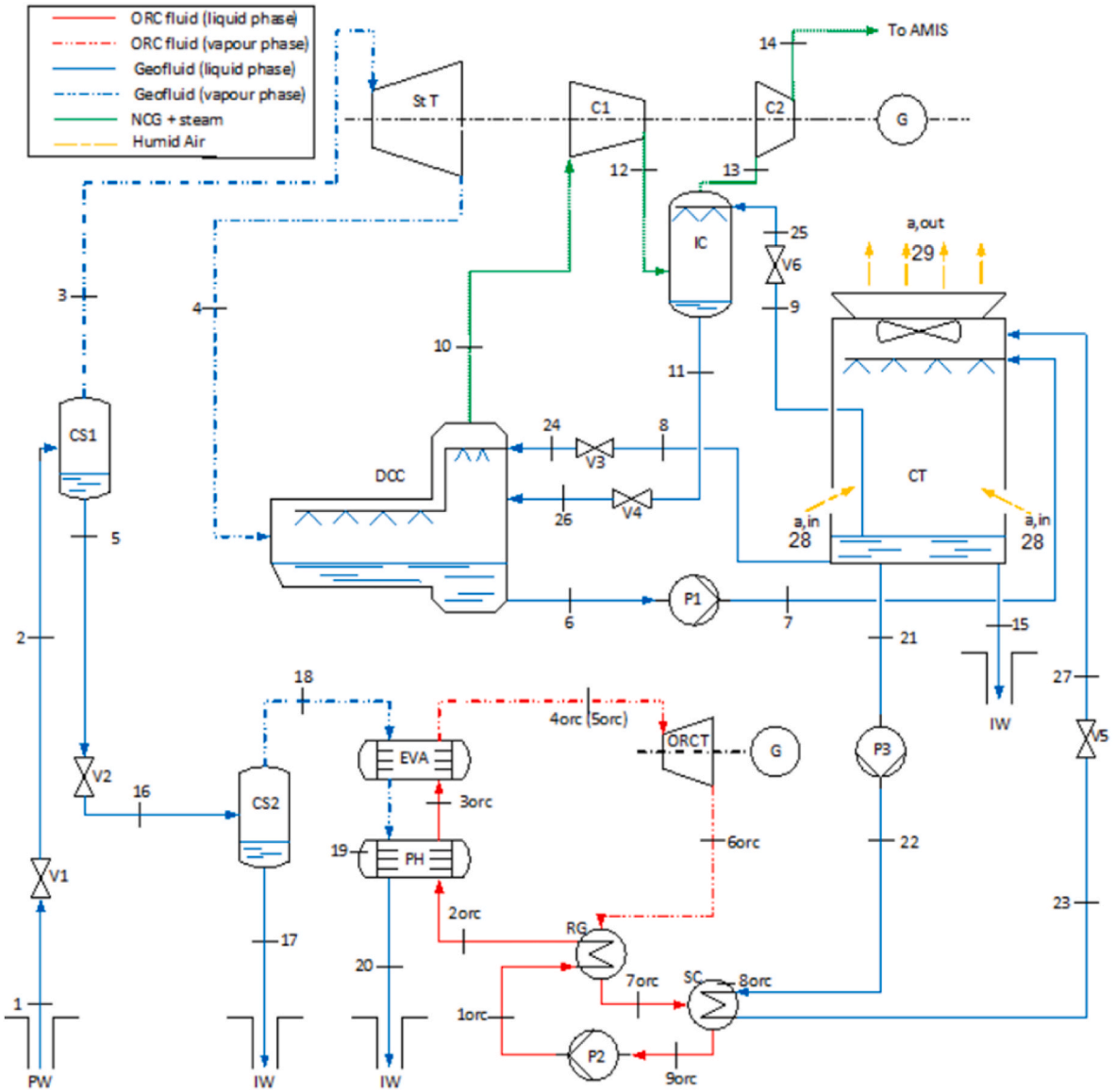

Fig. 1. Schematic of Bagnore 3 power plant [53].

at suitable depth, coupled to an advanced (supercritical) binary cycle.

The aim of this study is therefore to **evaluate the energy, exergy and economic performance** of the proposed advanced CO_2 power plant, which guarantee a relevant step ahead in the environmental behaviour of the geothermal powerplants, but they could result into a not economically viable options if compared to the current single and double flash technologies. Therefore, the investigation and comparison of optimized solutions adopting supercritical CO_2 cycles configurations to the selected case study, in order to assess the *most suitable ones to compete with the current single flash + ORC power plant,* either from thermodynamic and exergo-economic points of view, is relevant in order to assess the suitability of this possible alternative solution. Fig. 1 presents the schematic of the current power plant and Table 1 summarizes its main performance parameters.

2. Methodology

2.1. Mt. Amiata case study – borehole pump

The Amiata geothermal field was selected as a case study because of the difficulties encountered in using the local resource with flash power plant technology. The brine is particularly rich in antimony sulphide (Stibnite), which precipitates in the flash drain at temperature below 140 °C and is responsible for the scaling of the ducts, causing drastic reductions of the passage sections. In order to prevent the scaling of Stibnite, the introduction of a borehole pump upstream the flash point located inside the well at 800 m depth from the ground level was proposed, thereby maintaining the geothermal fluid under pressurized liquid conditions, from the extraction to the re-injection reservoir. The required pump head and power were calculated modelling the friction and heat losses in the geothermal fluid extraction duct. The pressurized fluid, after having delivered its sensible heat to the working fluid, is re-injected at a fixed 150 °C temperature, in order to avoid any sedimentation of stibnite while ensuring, at the same time, a correct management of the geothermal field. A guideline applied in this research is to maintain the geothermal fluid under pressurized liquid conditions: this includes the modelling of the well thermo-fluid dynamics and of the borehole pump. A model was thus developed in EES [EES, 2020] in order to calculate the heat transfer and pressure losses, while the fluid (geothermal brine in liquid conditions) is ascending the well duct. A steel cladding is included only in the first 500 m from the surface. Once the geometry is fixed, the head losses, which must be overcome by the borehole pump in order to maintain the geothermal fluid in liquid phase were calculated; the same was done for the heat losses. The Colebrook formula for the calculation of the friction factor was utilized. The temperature of the ground is assumed to vary linearly with a gradient of 50 °C per km of depth, from the starting value of the ambient temperature of 285 K.

Table 2 and Fig. 2 show the main thermodynamic and performance parameters and the configuration of the borehole pump respectively.

2.2. Power plants schematics and basic computational relationships

In this work, several power plant configurations were considered to evaluate the optimal power plant layout to be applied to the investigated medium temperature geothermal resource. Clearly, it is general for many different aspects, so that it may be representative of many other cases of exploitation of medium – high temperature geothermal resource with trans and supercritical CO_2 binary cycles. Fig. 3 displays the analysed configurations and Fig. 4 represents the corresponding temperature-entropy diagrams. Particularly, the assessed configurations include a recuperative cycle, a recuperative cycle with reheating, a recuperative cycle with reheating and intercooling, a precompression cycle, a recompression cycle with two recuperators and a recompression cycle with one recuperator. The increased complexity of the plant layout should be compensated by an increase in the system efficiency. The goal of this analysis was to test different plant configuration to asses whether this increase of efficiency is worth of, from an economic perspective, in a geothermal context.

Table 1
Bagnore 3 single flash + ORC power plant performance parameters.

Parameter	Value
First Law efficiency η	0.19
Second Law efficiency η_{II}	0.46
Net power output W_{net}	20 [MW]]wW
Cost of energy	0.04 [€/kWh]

Table 2
Main borehole pump parameters. The inlet condition of the pump is evaluated by modelling the well behaviour from the reservoir condition (T = 325 °C, P = 250 bar, from Ref. [53]) up to 800m where the pump is located.

Parameter	Value
η	0.8
W_{bp}	0.87 [MW]
T_{inBH}	273 [C]
P_{inBH}	5758 [kPa]
T_{outBH}	274.6 [C]
P_{outBH}	10258 [kPa]

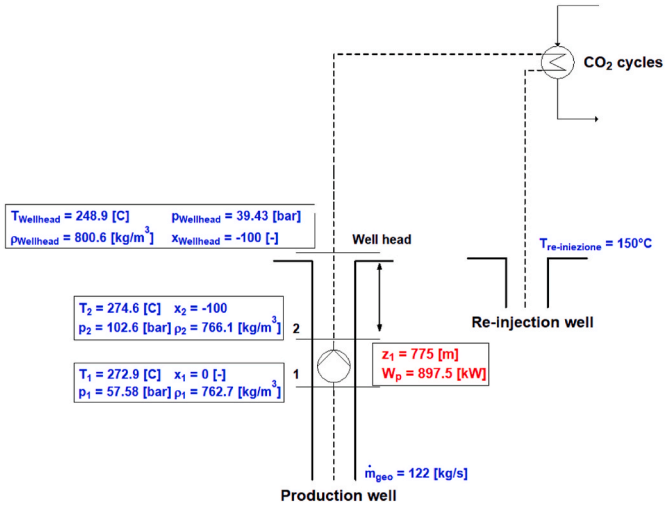

Fig. 2. Borehole pump schematic.

For each developed power plant, it was assumed that: (i) the cycles work in steady state conditions; (ii) the geothermal fluid is modelled as pure water; (iii) the difference in kinetic and potential energy between the input and output of turbomachines and heat exchangers is neglected; (iv) the isentropic efficiency of turbomachines is fixed. The real fluids thermodynamic properties were evaluated by EES internal libraries [65].

For each component, mass end energy balance equations were applied, as displayed in Eqns. (1) and (2).

$$\sum \dot{m}_{in} = \sum \dot{m}_{out} \tag{1}$$

$$\dot{W} + \dot{Q} = \sum \dot{m}_{out} h_{out} - \sum \dot{m}_{in} h_{in} \tag{2}$$

The first law efficiency was then defined as shown in Eq. (3).

$$\eta_I = \frac{\dot{W}_{net}}{\dot{Q}_{in}} \tag{3}$$

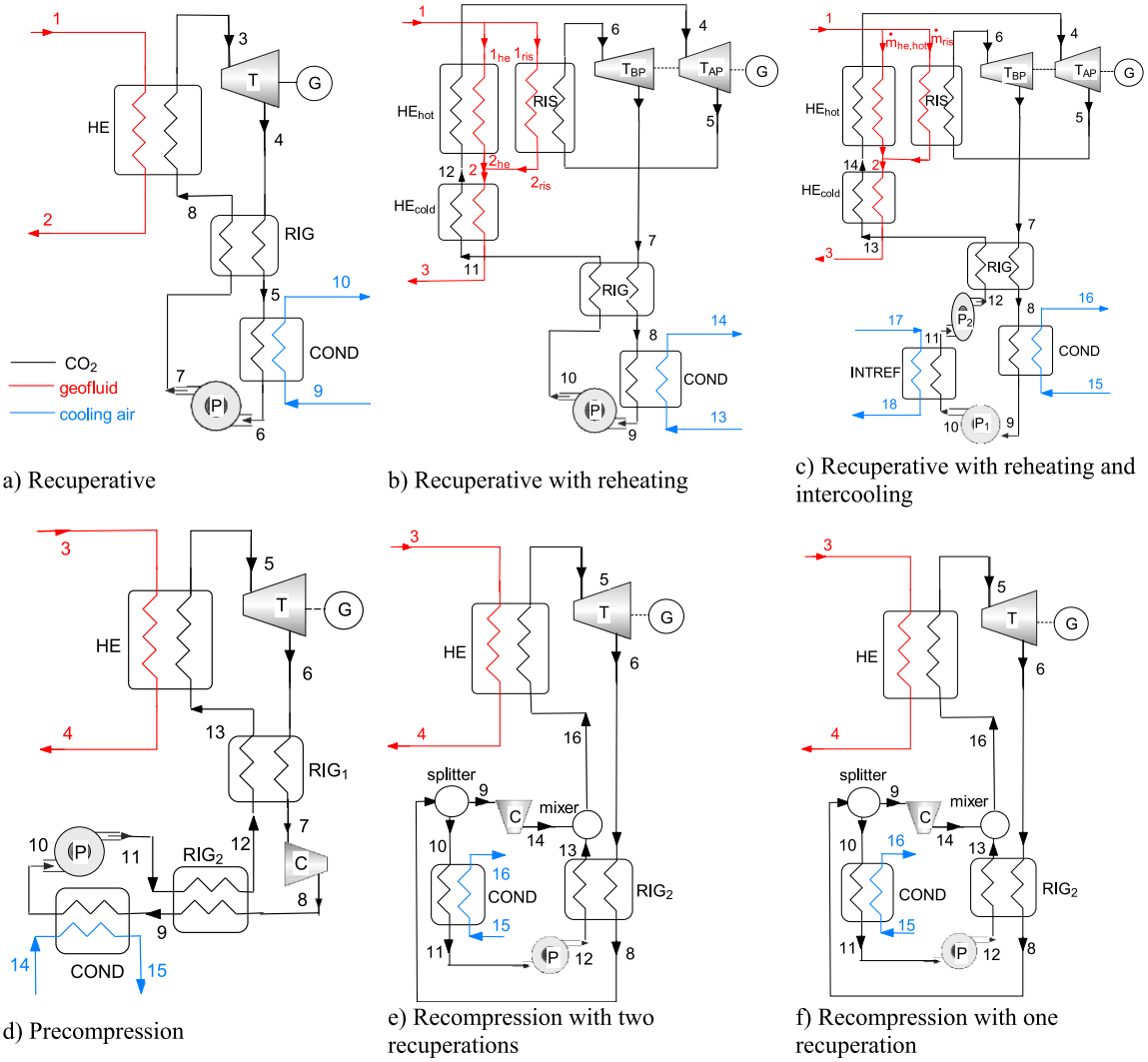

a) Recuperative

b) Recuperative with reheating

c) Recuperative with reheating and intercooling

d) Precompression

e) Recompression with two recuperations

f) Recompression with one recuperation

Fig. 3. Schematic of supercritical cycles.

while the Second law efficiency is defined in the following Eq. (4), direct and indirect expressions respectively:

$$\eta_{II} = \frac{\dot{W}_{net}}{\dot{m}_{Geo} \bullet (ex_{Geo\ in} - ex_{Geo\ out})} = 1 - \Sigma \mathrm{Exd}_{ri} - \Sigma \mathrm{Exl}_{ri} \tag{4}$$

where $ex_{Geo\ in}$ and $ex_{Geo\ out}$ are the specific exergies of geofluid at the inlet of borehole pump and outlet of the main geothermal heat exchanger, respectively. In the second expression, $\Sigma \mathrm{Exd}_{ri}$ and $\Sigma \mathrm{Exl}_{ri}$ are the sum of exergy destructions and losses of components, relative to the total exergy input to the system from the geothermal fluid (e.g. the denominator of the first expression).

2.3. Exergy and exergo-economic analysis

Exergy is the combination of the First and Second Laws of Thermodynamic, which allow to properly assess the energy efficiency of a system and to correctly identified the associated irreversibilities [54]. Exergy analysis is considered as one of the most robust method for the design and assessment of energy systems [55]. Indeed, the concept of exergy allows to estimate the effective thermodynamic values of energy flows. In the present work, the exergy is calculated at each point of the system by Eq (5).

$$\dot{E}x_j = \dot{m}_j \left[(h_j - h_o) - T_o (s_j - s_o) \right] \tag{5}$$

Combining the economic and exergy analysis(e.g. exergo-economic methodology) allows providing an efficient evaluation of the power plant and components cost-effectiveness, by introducing the costs per exergy unit [56]. The exergo-economic approach outlined in Ref. [57] was applied in this work by defining, for each component k, a cost balance equation, expressed in the following equation (6).

$$\dot{C}_{P,k} = \dot{C}_{F,k} + \dot{Z}_k \tag{6}$$

$$c_{P,k} \dot{E}x_{P,k} = c_{F,k} \dot{E}x_{F,k} + \dot{Z}_k$$

where.

- $\dot{C}_{P,k}$ and $\dot{C}_{F,k}$ are the cost rates associated with exergy products and fuels respectively
- $c_{P,k}$ and $c_{F,k}$ are the costs per unit of exergy of product or fuel respectively.
- $\dot{Z}_k$ is the sum of cost rates associated with investments and O&M for the k-th component.

In order to determine the investment and O&M costs ($\dot{Z}^{CI}_{tot} + \dot{Z}^{OM}_{tot}$) of the proposed power plants, an economic analysis was carried out. The cost functions applicable to the system components were obtained from Refs. [16,58]. Costs were actualized to 2019 values, by using the CEPCI indexes [66]. The Operation and Maintenance costs (O&M) of each

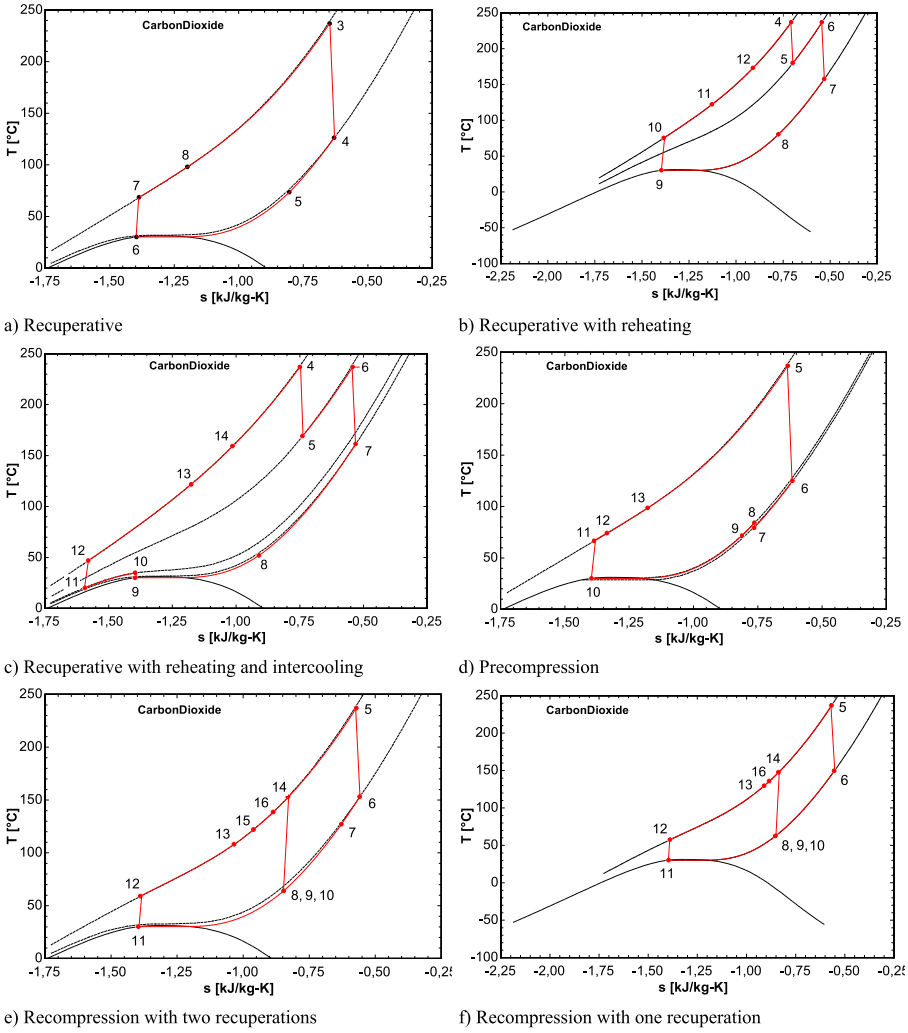

Fig. 4. T – s diagram of supercritical cycles.

component were determined following the best practises in literature [16,59].

Finally, Table 3 summarizes the exergo-economic balances and the auxiliary equations [56], which are logic statements that allow defining the missing number of conditions to solve the cost equations applied to each component for the recuperative cycle. The balances of the other configurations can be found in Appendix A.

Table 3
Exergo-economic balance equations of power plant components for the recuperative configuration.

	Recuperative
Borehole pump	$c_{21} \bullet \dot{E}x_{21} = c_{20} \bullet \dot{E}x_{20} + c_{W_{pkJ}} \bullet \dot{W}_{BHpump} + \dot{Z}_1 \quad c_{W_{pkJ}} = c_{W_{tkJ}}$ $c_{20} = c_{fuel_{kJ}}$
Condenser	$c_6 \bullet \dot{E}x_6 + c_{10} \bullet \dot{E}x_{10} = c_5 \bullet \dot{E}x_5 + c_9 \bullet \dot{E}x_9 + \dot{Z}_2 \; c_9 = 0 \; c_{10} = c_9$
Recuperator	$c_8 \bullet \dot{E}x_8 + c_5 \bullet \dot{E}x_5 = c_7 \bullet \dot{E}x_7 + c_4 \bullet \dot{E}x_4 + \dot{Z}_3 \; c_4 = c_5$
Heater$_{geo}$	$c_2 \bullet \dot{E}x_2 + c_3 \bullet \dot{E}x_3 = c_1 \bullet \dot{E}x_1 + c_8 \bullet \dot{E}x_8 + \dot{Z}_4 \; c_1 = c_{21} \bullet \frac{\dot{E}x_{21}}{\dot{E}x_1} c_1 = c_2$
Turbine	$c_{W_{tkJ}} \bullet \dot{W}_T + c_4 \bullet \dot{E}x_4 = c_3 \bullet \dot{E}x_3 + \dot{Z}_5 \; c_4 = c_3$
Compressor	$c_7 \bullet \dot{E}x_7 = c_6 \bullet \dot{E}x_6 + c_{W_{pkJ}} \bullet \dot{W}_{pump} + \dot{Z}_6$

3. Results

3.1. Power cycles optimization

The main parameters influencing the cycles efficiency are the maximum pressure and temperature. Specifically, a very wide range of maximum cycle pressures were investigated, with a wider range for the recuperative cycle with reheating and intercooling, in order to assess the optimal configuration of the power plants. On the other hand, the maximum temperature of the cycle was defined by the geothermal source at 249 °C, therefore the ΔT approach was varied in order to investigate its influence on both efficiency and cost. The main fixed parameters of the sCO_2 power cycles are summarized in the following bullets points.

- The CO_2 at condenser output is under saturated liquid conditions;
- The condenser range temperature and pinch point difference, $\Delta T_{range} = 10$ °C and $\Delta T_{pp} = 5$ °C respectively;
- Isentropic efficiency of turbines and compressors fixed at $\eta_t = 0.92$ and $\eta_c = 0.92$ respectively;
- Minimum hot/cold side temperature difference at recuperative heat exchangers $\Delta T_{min} = 10$ °C;
- Minimum pressure of power cycles $p_{min} = 7000$ kPa;
- Geofluid mass flowrate, temperature and pressure at borehole pump inlet $m_{Geo} = 122$ kg/s, $T_{Geo} = 272.9$ °C, $p_{Geo} = 5758$ kPa.

- Geofluid reinjection temperature $T_{rGeo} = 150$ °C;
- Reference environmental temperature and pressure $T_{amb} = 15$ °C and $p_{amb} = 101.325$ kPa respectively.

Fig. 5 shows the behaviour of the first law efficiency and unit electricity exergo-economic cost at variable maximum pressure (a and b) and ΔT approach (c and d) of the investigated power cycles configurations reported in Figs. 3 and 4. The figures clearly show that the recuperative configuration with reheating and intercooling is the highest efficiency one, followed by the recuperative and reheating configuration. For all the proposed cycles, an optimizing efficiency range of maximum pressure exists. It is essentially due to the variable shape of the cycles at different p_{max}, which is rather remarkable in the range of 15000–30000 kPa. On the other hand, the First Law efficiency and unit energy cost are less sensitive to ΔT approach, with the costs monotonically decreasing with increasing ΔT, due to the dominant effect of heat exchanger cost on the slightly improved performance at low ΔT. The efficiency of the cycles also shows a slight optimization at ΔT in the 3–8°, because of the increase of the compressors work for very low ΔT approach due to the increase of the area (and therefore of the pressure losses) of the heat exchanger.

Conversely to the efficiency behaviour, the lowest exergo-economic cost is achieved from the less efficient configuration which, however, is also the simplest one, namely the recuperative layout. This was expectable, as the other configurations allow indeed improved performance, but not so high to counterbalance the increased costs due to the additional required equipment. This is even more remarkable for the recompression configurations, allowing a modest increase of efficiency at the price of much larger exergo-economic costs. Another interesting feature of the recompression configurations, is their optimal efficiency at lower maximum pressures, while the recuperative and the precompression layouts require higher maximum pressure to achieve high cycle efficiencies and low exergo-economic costs.

The performance data of the optimized power cycles are summarized in Table 4. The considered configuration allows a 249 °C geothermal fluid temperature at the inlet of the main HE, also considering the temperature increase given by the pumping process. The geothermal fluid is re-injected at 150 °C in order to avoid the precipitation of stibnite while guaranteeing, at the same time, a correct management of the geothermal field. The best performing thermodynamic cycle is the recuperative with reheating and intercooling, which achieves an efficiency, even including the pumping power from the borehole pump and the heat losses of the ascending geothermal fluid in the well close to that of the currently installed single flash unit (19 %). However, the maximum achievable power output is much lower than the reference case, with a dramatic 40 % reduction in power output. Indeed, all the configurations loose an amount of power output between 40 and 50 % when compared to the traditional flash solutions.

The largest gross power production was achieved with the recompression cycles. However, these layouts have the main drawback of requiring the highest compressor power, exceeding 12 MW, which is almost double than all the other configurations. These ones, however, guarantee the lowest maximum pressure of the cycle at 18.9 and 18.6 [MPa] respectively, for the configurations 1 and 2 with recuperation. The performance levels of the considered powerplants layouts, when in configurations similar (in particular the recuperative one) to those proposed by Ref. [35,37], are comparable, considering the different thermodynamic working conditions.

Finally, the recuperative cycle is the one generating the lowest amount of power, and therefore it is also the less efficient one. It should be remarked that the considered overall power plant efficiency considers the heat losses in the ascending well pipe. If the analysis was carried out from the well-head input, the overall efficiency would be closer to the cycle efficiency, and therefore higher than the reference case with flash.

3.2. Exergy analysis: results

Fig. 6 shows the non-dimensional exergy destruction and losses of each component of the power cycles. The exergy input from the geothermal resource, was fixed at the same value for each thermodynamic cycle. As it is evident from Fig. 6a, the highest exergy loss comes from the heat loss in the production well (29 %). Indeed, this loss is

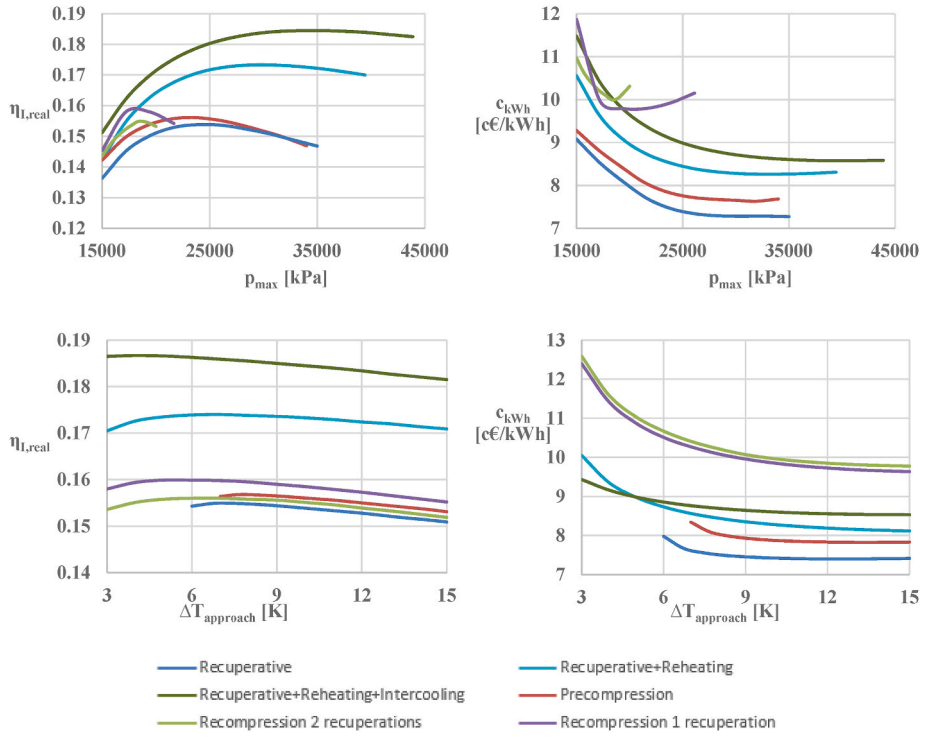

Fig. 5. Efficiency and produced energy unit cost as a function of max pressure and $\Delta T_{approach}$ with geothermal fluid.

Table 4
Performance comparison of each supercritical CO_2 cycle configuration.

Performance Parameter		Recuperative	Recuperative with reheating	Recuperative with reheating and intercooling	Precompression	Recompression with 2 recuperations	Recompression with 1 recuperation
Turbines	[kW]	17605	20053	20151	18138	23339	23926
Compressors	[kW]	6401	7545	6887.9	6784.7	12048	12371
Borehole pump	[kW]	873.2	873.2	873.2	873.2	873.2	873.2
Net Power	[kW]	10331	11635	12390	10480	10418	10682
Maximum Pressure	[kPa]	24931	30661	35171	23670	18976	18611
CO_2 Cycle Efficiency		[−]	0.2414	0.2559	0.2191	0.2179	0.223
Global Power Plant Efficiency		[−]	**0.1733**	**0.1845**	**0.1561**	**0.1552**	**0.1591**

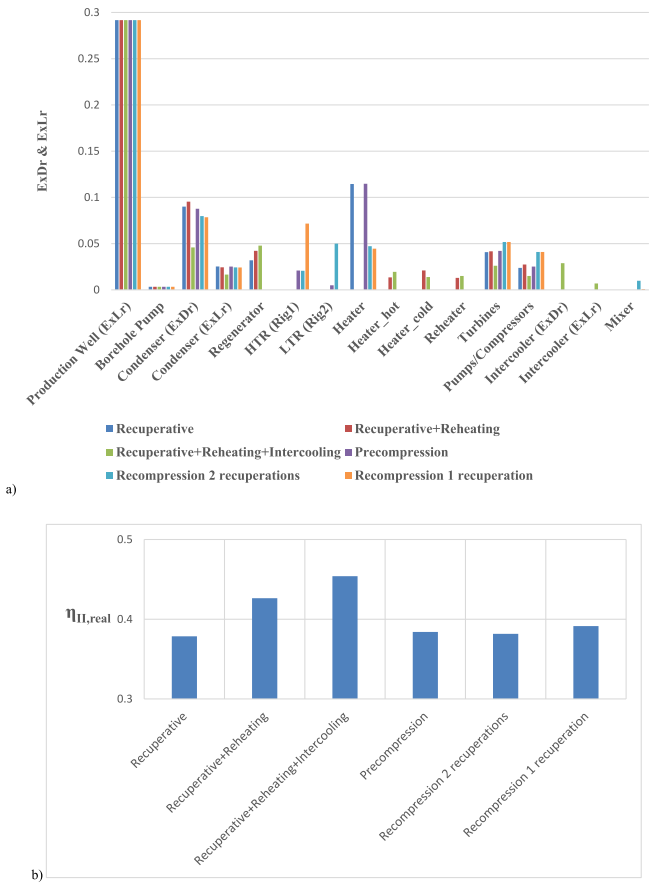

Fig. 6. a) Comparison of components exergy destruction of the different configurations overall; b) Comparison of overall Second Law efficiency of the different configurations.

common to all the considered cycles and cannot be avoided. On the other hand, the exergy losses at the condenser to the environment, are not the main contributors to the inefficiency of the cycles, as they are in the range of 2 %. These levels of losses are clearly related to the largely different exergy value of the two heat losses.

The source of highest exergy destruction is differently located for the considered cycles: for example, in the recuperative and precompression cycles the highest values belong to the main heater (HE). Furthermore, the exergy destructions in the condenser represent the second main contributor to the inefficiency of the cycles, with values higher than 7.5 % for all the configurations except the recuperative one with reheat and intercooling, as it allows a further heat recuperation from the exhaust stream of the turbine.

From the sum of the exergy destructions, it is possible to address the best and worst performing power cycles configurations. The highest exergy efficiency (45.4 %) belongs to the recuperative cycle with reheat and intercooling, as clearly shown on Fig. 6b. Again, this value is in line with those found on [35] for similar configurations, taking into account of the different thermodynamic conditions. As clear from the comparison of the exergy destruction sources in the different cycles, this is mainly due to the lower values found in the heaters and the condenser. Moreover, the good coupling of the fluids heat capacities (water and CO_2) allows achieving a satisfactory value of exergy efficiency in the main HE for this power plant layout. On the contrary, for the same reason (e.g. the weak coupling of heat capacities in the main HE) the recuperative cycle configuration shows the lowest overall value of exergy efficiency.

3.3. Exergo-economic analysis: results

The cost of electricity generation for the proposed power plant configuration can be obtained from an exergo-economic assessment. The levelized cost of electricity for geothermal power plants project installed (or in progress) between 2007 and 2021 varies depending on technology and size. Particularly, for binary cycle configuration the cost of electricity varies between 4 c€/kWh for very big power plants (>300 MW), to values close to 14 c€/kWh for power plants with a nominal capacity of 1 MW. The mean range for electricity production from geothermal power plants is between 6 and 10 c€/kWh [67].

The Purchase Equipment Costs (PEC) of the power cycles components, achieved from the functions available in Refs. [16,58] and actualized to 2019 values, by using the CEPCI indexes [66], are summarized in Table 5. The recuperative with reheat only configuration is included into the Recuperative + RH + IC.

The other costs were assumed as a reasonable fraction of total PEC for all configurations, namely.

- Total purchased equipment installation costs = 6 % PEC;
- Piping costs = 7 % PEC;
- Instrumentation, control and electrical equipment costs = 5 % PEC;
- Civil work costs = 7 % PEC;
- Engineering and supervision costs = 6 % PEC;
- Construction costs = 3 % PEC;
- Contingency costs = 8 % PEC;
- Working capital costs = 3 % PEC;
- Maintenance costs = 1.5 % Total Capital Investment (TCI);
- Insurance costs = 1.5 % Total Capital Investment (TCI).

In the here presented power plant case studies, the range of installed power is between 10 and 15 MW. These lead to a relatively high cost of electricity for some configurations (recompression), but still very close or in line with the expected electricity production values. Particularly, the lowest electricity cost (7.42 c€/kWh) was achieved with the recuperative configuration. In a similar configuration proposed by Ref. [35], in the 1 MW size range but with geothermal resource temperature drop between 170 and 20 °C, 12 c$/kWh were achieved. Despite the here proposed one order of magnitude larger size and the higher maximum

Table 5
PEC of components for the different analysed power cycles.

Recuperative		Recuperative + RH + IC		Precompression		Recompression+1 REC		Recompression+2 REC	
Comp.	**PEC** [M€]	**Comp**	**PEC** [M€]	**Comp**	**PEC** [M€]	**Comp.**	**PEC** [M€]	**Comp.**	**PEC** [M€]
BH Pump	0.922	BH Pump	0.922	BH Pump	0.922	BH Pump	0.922	BH Pump	0.922
Condens.	5.83	Condens.	3.61	Condens.	5.83	Condens.	5.68	Condens.	5.71
RH	1.84	RIG	2.65	RCP	2.27	LTR	6.86	HTR	2.14
HE	2.53	HE hot	1.65	interRCP	0.964	HE	6.45	LTR	4.76
Turbine	3.34	HE cold	0.649	HE	2.82	Turbine	3.25	HE	5.80
Pump	1.90	RIS	3.14	Turbine	3.33	Compr. 1	1.56	Turbine	3.26
		Turb. HP	3.38	Compr.1	1.84	Compr. 2	2.12	Compr. 1	1.59
		Turb. LP	3.39	Compr. 2	0.440	Mixer 2		Compr. 2	2.04
		Pump 1	0.294						
		Pump 2	1.90						
		IC	5.22						

temperature, considering the narrower geothermal resource temperature drop (e.g. 235–150 °C) the achieved cost of electricity can be considered very interesting. On the contrary, the highest electricity cost (9.98 c€/kWh) was obtained for the recompression cycle layout with one recuperation. The configuration achieving the highest efficiency (recuperative with reheating and intercooling) is at 8.6 €/kWh electricity cost level, which is however a proper value for this power range. Anyhow, comparing the obtained electricity costs with that of the reference power plant (Bagnore 3, single flash + ORC), the costs of sCO_2 binary cycles are double. Nonetheless, this kind of power plants can be attractive, as they could guarantee and almost zero environmental impact configuration during the operation phase. Fig. 7 summarizes the calculated electricity cost for all the analysed power cycles.

3.4. Influence of heat exchangers pressure losses on cycles performance and electricity cost

Finally, given the primary importance of the heat exchangers performance, size and cost on the cycle efficiency and electricity cost, the influence of the pressure losses of the heat exchangers was carried out. In fact, when dealing with heat exchangers network in power cycles, it is well known the counteracting effects of their efficiency, generally enhanced with high specific area per unit volume, with the induced higher pressure losses, which negatively affect the cycle performance. Indeed, here the recent very efficient and compact Printed Circuit Heat Exchangers (PCHE, [60,61]) were adopted, so deserving an accurate addressing of the pressure losses against their high heat transfer performance. The results presented so far included the evaluation of the pressure losses within the circuit, calculated through the developed model of the heat exchangers (see the models reported in Appendix B). With the correlations reported in Appendix B for the different PCHEs, the related pressure drops have been calculated with the Darcy-Weisbach relationships as follows:

$$\Delta p_c = f_c \bullet L_{channel} \bullet \frac{v_c^2}{2} \bullet \frac{\rho_c}{2Dh} \text{ cold fluid side;} \quad (5)$$

$$\Delta p_h = f_h \bullet L_{channel} \bullet \frac{v_h^2}{2} \bullet \frac{\rho_h}{2Dh} \text{ hot fluid side.} \quad (6)$$

The influence of the heat exchangers pressure losses is, on the whole, not negligible, as they reduce the efficiency in a relevant amount, especially for the recompression cycles where the efficiency drops by almost 5 percentage points, as clear from Fig. (8). The calculated levels of PCHEs pressure drops are in line with those found on [37] for similar geometries. In the present analysis, the Authors considered PCHEs with semicircular cross-section channels, even though very recently the superior characteristics of triangular [39] and star shaped [64] cross-section channels were addressed.

The drop in efficiency is directly related to the increase of the produced electricity cost. Indeed, as can be grasped from Fig. (9), the associated increase of the produced electricity cost is more remarkable for the recompression cycles, due to the relevant decrease in efficiency due to friction pressure losses, leading to an increase of costs of more than 1 c€/kWh. On the other hand, the lowest increase in electricity cost due to HX pressure losses belongs to the recuperative cycle

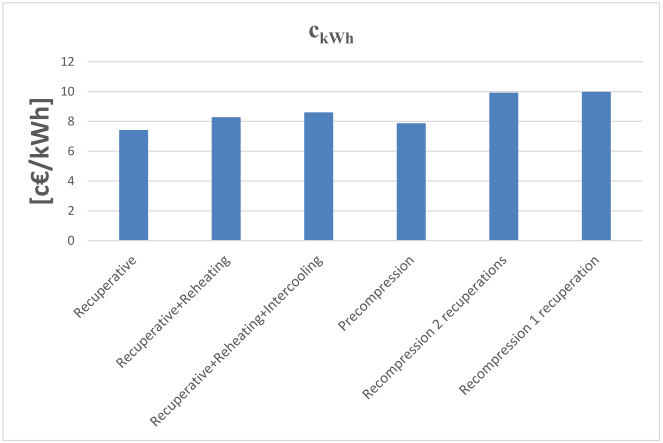

Fig. 7. Comparison of electricity costs for the analysed power plants.

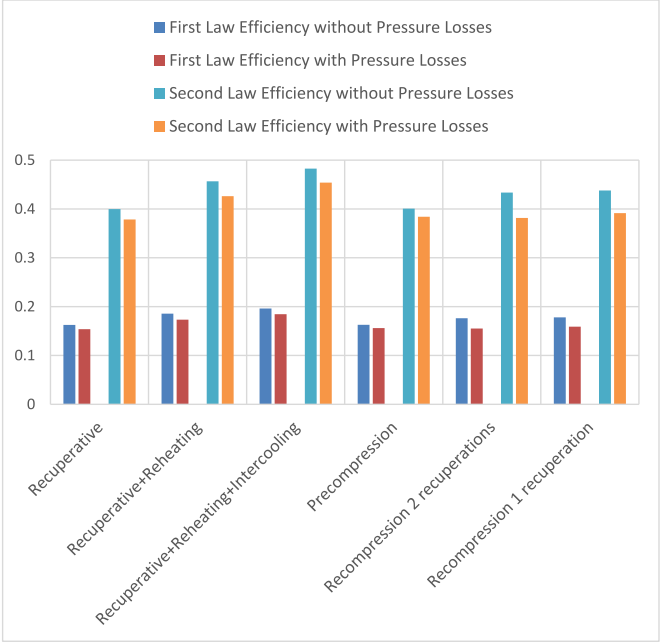

Fig. 8. Sensitivity of first and second low efficiencies of the proposed cycles to the pressure losses in the heat exchangers (bars with and without considering them).

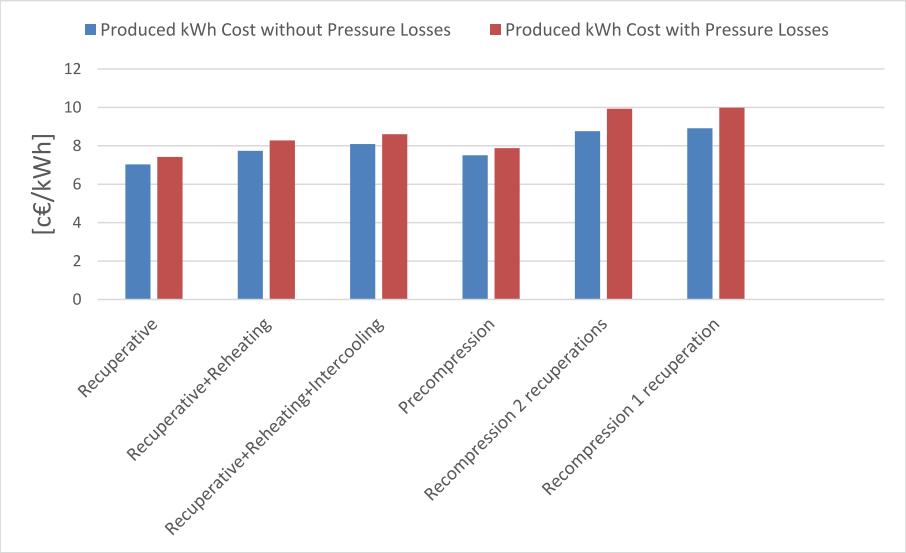

Fig. 9. Sensitivity of electricity cost of the proposed cycles to the pressure losses in the heat exchangers (bars with and without considering them).

configuration, as it is the simplest one from this point of view.

4. Conclusions

In this study an exergo-economic assessment of different supercritical CO_2 power cycles configurations for the exploitation of water dominant geothermal resources in place of traditional flash based technologies was carried out by the means of energy, exergy and exergo-economic analysis. The proposed power cycle configurations adopted the efficient PCHE which, on the other hand, may negatively affect the cycle performance due to their possible relevant pressure losses. The results confirmed that the supercritical CO_2 cycles may be valuable binary cycles solutions for the exploitation of low temperature geothermal resources, as the produced cost of electricity is in line with the existing binary cycle costs [67].

The most remarkable outcomes from the present research are the costs of electricity related to the adoption of supercritical power cycles under six different configurations, exploiting the same fixed geothermal resource.

- The lowest cost of electricity was achieved for the simplest recuperative cycle configurations, at 7.4 c€/kWh, which is in line with the level of current geothermal binary cycles.
- The configuration allowing the highest thermodynamic efficiency was the recuperative with intercooling and reheating, which gave First and Second Law efficiencies of 18.5 % and 45.5 % respectively. However, due to the increase in complexity of the power plant configurations, especially related to the "heavier" heat exchangers network, the cost of electricity becomes slightly higher (8.092 c€/kWh), even though still competitive with that of current binary cycles.
- The recompression configurations are hindered by the high required compressors work, having therefore the highest produced electricity costs and the lowest efficiencies. Nonetheless, it should be remarked that these configurations guarantee the lowest maximum cycles pressures (around 190 bar).
- All the binary configurations show lower performance when compared to the currently adopted single flash + ORC power cycle, with a reduction of the power output in the range of 40–50 % and an almost doubled cost of the electricity. On the other hand, these CO_2 power plants could guarantee an almost zero environmental impact during the operation phase.

As a concluding remark, this analysis well addresses the importance of including the effect of pressure losses in the heat exchangers, also considering the fact that the high efficiency and compact PCHE were adopted, where this issue may be typically relevant. It is shown, here, that this aspect might lead to a significant increase of the produced electricity costs, related to the entailed drop of power cycles efficiency, especially in the most complex configurations.

The results of this research introduce, in the context of known configurations of CO_2 based binary cycles to exploit geothermal resources, the novelties related to two main aspects which are missing in literature.

1) The accurate evaluation and comparison of electricity production costs by the means of exergo-economic methodology;
2) This methodology was applied to cycles equipped with PCHEs which is a novel proposal in these applications, particularly for the aspects addressing the influence of the related pressure losses on the cycle's performance.

CRediT authorship contribution statement

N. Di Michele: Writing – original draft, Validation, Software, Data curation. **L. Talluri:** Supervision, Formal analysis, Data curation. **P. Ungar:** Validation, Investigation. **D. Fiaschi:** Writing – review & editing, Supervision, Project administration, Funding acquisition, Conceptualization.

Declaration of competing interest

The authors declare that they have no known competing financial interests or personal relationships that could have appeared to influence the work reported in this paper.

Acknowledgments

The present research was partially supported by the European Commission H2020 Program, GA Nr 963530 (*LEAP-RE JA Project, WP9 Geothermal Atlas for Africa*) and partially funded under the National Recovery and Resilience Plan (NRRP), Mission 4 Component 2 Investment 1.3 - Call for tender No. 1561 of October 11, 2022 of Ministero dell'Università e della Ricerca (MUR); funded by the European Union – NextGenerationEU, Contract nr PE0000021.

AppendixA

Exergo-economic balance equations of power plant components for the assessed configurations.

	Recuperative with reheating	Recuperative with reheating and intercooling	Precompression	Recompression with two recuperations	Recompression with one recuperation
Borehole pump	$c_{21}\bullet\dot{Ex}_{21}=c_{20}\bullet\dot{Ex}_{20}+c_{Wp_{kJ}}\bullet\dot{W}_{BHpump}+\dot{Z}_1$ $c_{Wp_{kJ}}=c_{Wt_{kJ}}$ $c_{20}=c_{fuel_{kJ}}$	$c_{21}\bullet\dot{Ex}_{21}=c_{20}\bullet\dot{Ex}_{20}+c_{Wp_{kJ}}\bullet\dot{W}_{BHpump}+\dot{Z}_1$ $c_{Wp_{kJ}}=c_{Wt_{kJ}}$ $c_{20}=c_{fuel_{kJ}}$	$c_{21}\bullet\dot{Ex}_{21}=c_{20}\bullet\dot{Ex}_{20}+c_{Wp_{kJ}}\bullet\dot{W}_{BHpump}+\dot{Z}_1$ $c_{Wp_{kJ}}=c_{Wt_{kJ}}$ $c_{20}=c_{fuel_{kJ}}$	$c_{21}\bullet\dot{Ex}_{21}=c_{20}\bullet\dot{Ex}_{20}+c_{Wp_{kJ}}\bullet\dot{W}_{BHpump}+\dot{Z}_1$ $c_{Wp_{kJ}}=c_{Wt_{kJ}}$ $c_{20}=c_{fuel_{kJ}}$	$c_{21}\bullet\dot{Ex}_{21}=c_{20}\bullet\dot{Ex}_{20}+c_{Wp_{kJ}}\bullet\dot{W}_{BHpump}+\dot{Z}_1$ $c_{Wp_{kJ}}=c_{Wt_{kJ}}$ $c_{20}=c_{fuel_{kJ}}$
Condenser	$c_9\bullet\dot{Ex}_9+c_{14}\bullet\dot{Ex}_{14}=c_8\bullet\dot{Ex}_8+c_{13}\bullet\dot{Ex}_{13}+\dot{Z}_2$ $c_{13}=0$ $c_{14}=c_{13}$	$c_9\bullet\dot{Ex}_9+c_{16}\bullet\dot{Ex}_{16}=c_8\bullet\dot{Ex}_8+c_{15}\bullet\dot{Ex}_{15}+\dot{Z}_2$ $c_{15}=0$ $c_{16}=c_{15}$	$c_{10}\bullet\dot{Ex}_{10}+c_{15}\bullet\dot{Ex}_{15}=c_9\bullet\dot{Ex}_9+c_{14}\bullet\dot{Ex}_{14}+\dot{Z}_2$ $c_{14}=0$ $c_{15}=c_{14}$	$c_{11}\bullet\dot{Ex}_{11}+c_{18}\bullet\dot{Ex}_{18}=c_{10}\bullet\dot{Ex}_{10}+c_{17}\bullet\dot{Ex}_{17}+\dot{Z}_2$ $c_{17}=0$ $c_{18}=c_{17}$	$c_{11}\bullet\dot{Ex}_{11}+c_{18}\bullet\dot{Ex}_{18}=c_{10}\bullet\dot{Ex}_{10}+c_{17}\bullet\dot{Ex}_{17}+\dot{Z}_2$ $c_{17}=0$ $c_{18}=c_{17}$
Recuperator	$c_{11}\bullet\dot{Ex}_{11}+c_8\bullet\dot{Ex}_8=c_{10}\bullet\dot{Ex}_{10}+c_7\bullet\dot{Ex}_7+\dot{Z}_3$ $c_7=c_8$	$c_{13}\bullet\dot{Ex}_{13}+c_8\bullet\dot{Ex}_8=c_{12}\bullet\dot{Ex}_{12}+c_7\bullet\dot{Ex}_7+\dot{Z}_3$ $c_7=c_8$	Rig1 $c_{13}\dot{Ex}_{13}+c_7\bullet\dot{Ex}_7=c_{12}\bullet\dot{Ex}_{12}+c_6\bullet\dot{Ex}_6+\dot{Z}_3$ $c_6=c_7$ Rig2 $c_{12}\dot{Ex}_{12}+c_9\bullet\dot{Ex}_9=c_{11}\bullet\dot{Ex}_{11}+c_8\bullet\dot{Ex}_8+\dot{Z}_4$ $c_8=c_9$	Rig1 $c_{16}\dot{Ex}_{16}+c_7\bullet\dot{Ex}_7=c_{15}\bullet\dot{Ex}_{15}+c_6\bullet\dot{Ex}_6+\dot{Z}_3$ $c_6=c_7$ Rig2 $c_8\dot{Ex}_8+c_{13}\bullet\dot{Ex}_{13}=c_{12}\bullet\dot{Ex}_{12}+c_7\bullet\dot{Ex}_7+\dot{Z}_4$ $c_7=c_8$	$c_8\bullet\dot{Ex}_8+c_{13}\bullet\dot{Ex}_{13}=c_6\bullet\dot{Ex}_6+c_{12}\bullet\dot{Ex}_{12}+\dot{Z}_3$ $c_6=c_8$
Heater_{geo}	Heater-hot $c_2{*}\dot{Ex}_{hehot2}+c_4{*}\dot{Ex}_4=c_1{*}\dot{Ex}_{hehot1}+c_{12}{*}\dot{Ex}_{12}+\dot{Z}_4$ $c_1=c_{21}{*}\frac{\dot{Ex}_{21}}{\dot{Ex}_1}$ $c_1=c_2$ Heater-cold $c_3{*}\dot{Ex}_3+c_{12}{*}\dot{Ex}_{12}=c_2{*}\dot{Ex}_2+c_{11}{*}\dot{Ex}_{11}+\dot{Z}_5$ $c_2=c_3$	Heater-hot $c_2{*}\dot{Ex}_{hehot2}+c_4{*}\dot{Ex}_4=c_1{*}\dot{Ex}_{hehot1}+c_{14}{*}\dot{Ex}_{14}+\dot{Z}_4$ $c_1=c_{21}{*}\frac{\dot{Ex}_{21}}{\dot{Ex}_1}$ $c_1=c_2$ Heater-cold $c_3{*}\dot{Ex}_3+c_{14}{*}\dot{Ex}_{14}=c_2{*}\dot{Ex}_2+c_{13}{*}\dot{Ex}_{13}+\dot{Z}_5$ $c_2=c_3$	$c_4{*}\dot{Ex}_4+c_5{*}\dot{Ex}_5=c_3{*}\dot{Ex}_3+c_{13}{*}\dot{Ex}_{13}+\dot{Z}_5$ $c_3=c_{21}{*}\frac{\dot{Ex}_{21}}{\dot{Ex}_3}$ $c_3=c_4$	$c_4{*}\dot{Ex}_4+c_5{*}\dot{Ex}_5=c_3{*}\dot{Ex}_3+c_{16}{*}\dot{Ex}_{16}+\dot{Z}_5$ $c_3=c_{21}{*}\frac{\dot{Ex}_{21}}{\dot{Ex}_3}$ $c_3=c_4$	$c_4{*}\dot{Ex}_4+c_5{*}\dot{Ex}_5=c_3{*}\dot{Ex}_3+c_{16}{*}\dot{Ex}_{16}+\dot{Z}_4$ $c_3=c_{21}{*}\frac{\dot{Ex}_{21}}{\dot{Ex}_3}$ $c_3=c_4$
Reheater	$c_2{*}\dot{Ex}_{ris2}+c_6{*}\dot{Ex}_6=c_1{*}\dot{Ex}_{ris1}+c_5{*}\dot{Ex}_5+\dot{Z}_6$	$c_2{*}\dot{Ex}_{ris2}+c_6{*}\dot{Ex}_6=c_1{*}\dot{Ex}_{ris1}+c_5{*}\dot{Ex}_5+\dot{Z}_6$			
Turbine	Turbine_{AP} $c_{Wt_{ApkJ}}\dot{W}_{TAP}+c_5\dot{Ex}_5=c_4\bullet\dot{Ex}_4+\dot{Z}_7$ $c_5=c_4$ Turbine_{BP} $c_{Wt_{BPkJ}}\dot{W}_{TBP}+c_7\bullet\dot{Ex}_7=c_6\bullet\dot{Ex}_6+\dot{Z}_8$ $c_7=c_6$ $c_{Wt_{kJ}}=\left(c_{Wt_{ApkJ}}\dot{W}_{TAP}+c_{Wt_{BPkJ}}\bullet\dot{W}_{TBP}\right)/(\dot{W}_{TAP}+\dot{W}_{TBP})$	Turbine_{AP} $c_{Wt_{ApkJ}}\dot{W}_{TAP}+c_5\bullet\dot{Ex}_5=c_4\bullet\dot{Ex}_4+\dot{Z}_7$ $c_5=c_4$ Turbine_{BP} $c_{Wt_{BPkJ}}\dot{W}_{TBP}+c_7\bullet\dot{Ex}_7=c_6\bullet\dot{Ex}_6+\dot{Z}_8$ $c_7=c_6$ $c_{Wt_{kJ}}=\left(c_{Wt_{ApkJ}}\bullet\dot{W}_{TAP}+c_{Wt_{BPkJ}}\bullet\dot{W}_{TBP}\right)/(\dot{W}_{TAP}+\dot{W}_{TBP})$	$c_{Wt_{kJ}}\dot{W}_T+c_6\bullet\dot{Ex}_6=c_5\bullet\dot{Ex}_5+\dot{Z}_6$ $c_5=c_6$	$c_{Wt_{kJ}}\bullet\dot{W}_T+c_6\bullet\dot{Ex}_6=c_5\bullet\dot{Ex}_5+\dot{Z}_6$ $c_5=c_6$	$c_{Wt_{kJ}}\bullet\dot{W}_T+c_6\bullet\dot{Ex}_6=c_5\bullet\dot{Ex}_5+\dot{Z}_5$ $c_5=c_6$
Compressor	$c_{10}\bullet\dot{Ex}_{10}=c_9\bullet\dot{Ex}_9+c_{Wp_{kJ}}\bullet\dot{W}_{pump}+\dot{Z}_9$	Compressor1 $c_{10}\bullet\dot{Ex}_{10}=c_9\bullet\dot{Ex}_9+c_{Wp_{kJ}}\bullet\dot{W}_{pump1}+\dot{Z}_9$ Compressor2 $c_{12}\bullet\dot{Ex}_{12}=c_{11}\bullet\dot{Ex}_{11}+c_{Wp_{kJ}}\bullet\dot{W}_{pump2}+\dot{Z}_{10}$	Compressor1 $c_{11}\bullet\dot{Ex}_{11}=c_{10}\bullet\dot{Ex}_{10}+c_{Wp_{kJ}}\bullet\dot{W}_{pump}+\dot{Z}_7$ Compressor2 $c_8\bullet\dot{Ex}_8=c_7\bullet\dot{Ex}_7+c_{Wp_{kJ}}\bullet\dot{W}_{comp}+\dot{Z}_8$	Compressor1 $c_{12}\bullet\dot{Ex}_{12}=c_{11}\bullet\dot{Ex}_{11}+c_{Wp_{kJ}}\bullet\dot{W}_{pump}+\dot{Z}_7$ Compressor2 $c_{14}\bullet\dot{Ex}_{14}=c_9\bullet\dot{Ex}_9+c_{Wp_{kJ}}\bullet\dot{W}_{comp}+\dot{Z}_8$	Compressor1 $c_{12}\bullet\dot{Ex}_{12}=c_{11}\bullet\dot{Ex}_{11}+c_{Wp_{kJ}}\bullet\dot{W}_{pump}+\dot{Z}_6$ Compressor2 $c_{14}\bullet\dot{Ex}_{14}=c_9\bullet\dot{Ex}_9+c_{Wp_{kJ}}\bullet\dot{W}_{comp}+\dot{Z}_7$
Intercooler		$c_{11}\bullet\dot{Ex}_{11}+c_{18}\bullet\dot{Ex}_{18}=c_{10}\bullet\dot{Ex}_{10}+c_{17}\bullet\dot{Ex}_{17}+\dot{Z}_{11}$ $c_{17}=0$ $c_{18}=c_{17}$			

Appendix B

Printed Circuit Heat Exchanger (PCHE) modelling

PCHE of the straight-channels type have been used for the Heaters, while for the recuperators the zigzag-channels type was selected. The channels, photochemically engraved on the plates, have a semi-circular section with a diameter D of 1.2 mm. The number of channels per fluid is determined by fixing the speed of the CO_2 flow and knowing the values of the mass flow rate, the average density of the fluid and the section area A of the single channel:

$$N_{channels}=\frac{\dot{m}_{CO_2}}{\overline{\rho}_{CO_2}v_{CO_2}A}$$

The number of channels and plates is the same for both fluids, therefore: $N_{channels_{tot}}=2N_{channels}$, $N_{plates_{tot}}=2N_{plates}$. The number of total plates of the heat exchanger has been chosen equal to the number of channels per plate:

$$N_{plates_{tot}}=N_{channels\ per\ plate}$$

$$N_{channels} = N_{channels\ per\ plate} \bullet N_{plates}$$

$$N_{plates} = \sqrt{\frac{N_{channels}}{2}}$$

It has also been assumed that wall temperatures are the average of the average temperatures of each fluid:

$$T_w = \frac{\overline{T}_{hotfluid} + \overline{T}_{coldfluid}}{2}$$

Heater

The relationships to obtain the convective heat exchange coefficient h were taken from [60].

Geofluid side (evaluated as pure water):

$$Nu = 0.122 Re^{0.56}\ Pr^{0.14}$$

$$f = (1.12 \ln(Re) + 0.85)^{-2}$$

CO_2 side:

$$Nu = Nu_{fc} f(B)$$

Where, for supercritical CO_2: $f(B) = 0.36 - 22\left(\frac{Gr}{Re^{2.7}}\right)^{0.42}$, for $T_w > T_{pc}$ and $3 \times 10^4 < Re < 7 \times 10^4$.

$$Nu_{fc} = 0.0183 Re^{0.82}\ Pr^{0.5} \left(\frac{\overline{\rho}_{CO_2}}{\rho_w}\right)^{-0.3}$$

$$Gr = \frac{(\overline{\rho}_{CO_2} - \overline{\rho}_w)\overline{\rho}_{CO_2} g D_h^3}{\overline{\mu}_{CO_2}^2}$$

$$\overline{\rho}_w = \frac{\overline{\rho}_{CO_2}(\overline{T}_{CO_2} - T_{pc}) + \rho_w(T_{pc} - T_w)}{(\overline{T}_{CO_2} - T_w)}$$

To assess the friction factor on the CO_2 side, Colebrook's formula was used, using $\varepsilon = 5\ \mu m$ as the roughness value for the channels [60].

Recuperator

The correlations in order to evaluate the convective heat transfer coefficient h were taken from Ref. [61]. The angle of inclination of the channels (zig-zag channels type) is chosen equal to $\alpha = 30°$. The correlations valid for CO_2 on both the cold and hot side with $3 \times 10^3 < Re < 2.6 \times 10^4$ are:

$$Nu = 0.0176 Re^{0.809}\ Pr^{1/3}$$

$$f = 0.3905 Re^{-0.0355}$$

The convective heat transfer coefficient is therefore: $h = \frac{Nu \bullet \overline{k}}{D_h}$.

Once the coefficients for both the cold fluid and the hot fluid have been found, the thermal resistance can be evaluated:

$R_{coldfluid} = \frac{1}{h_{coldfluid} S}$; $R_{hotfluid} = \frac{1}{h_{hotfluid} S}$; $R_{cond} = \frac{1}{4 k_{steel} L_{channel} N_{channels}}$; where S is the heat exchange surface, k is the conductivity and $L_{channel}$ is the length of the channels.

It can be found: $UA = \frac{1}{R_{tot}}$, dove $R_{tot} = R_{coldfluid} + R_{hotfluid} + R_{cond}$.

Knowing the inlet and outlet temperatures of the exchanger and the thermal capacities of the fluids, it is possible to evaluate through the method ε-NTU the value of $(UA)_{NTU}$. Therefore, the length of $L_{channel}$ is varied and an iterative process runs until $UA = (UA)_{NTU}$.

Mechanical design of PCHE

The mechanical design of the PCHE exchangers is taken from the article [63], figs. 14 and 15.

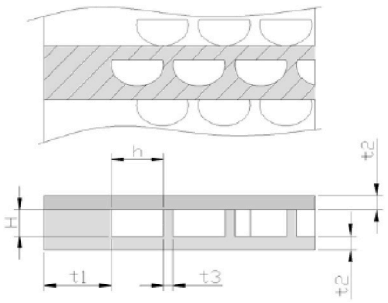

Fig. 14. simplified schematic of block geometry for mechanical design [63]

h = channel width
H = channel depth
t1 = edge width
t2 = wall thickness
t3 = ridge width

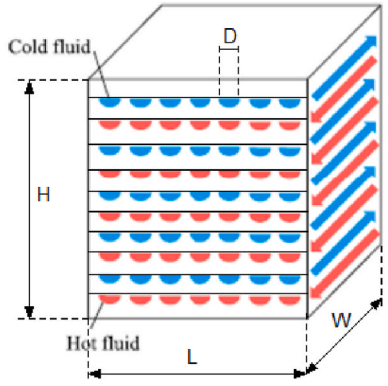

Fig. 15. schematic of PCHE stack [63]

It was assumed that $h = D$ e $H = \frac{D}{2}$.

$$t_1 > \frac{p_{max}D + \sqrt{p_{max}D^2(p_{max} + 7.5\sigma_{am}E)}}{6\sigma_{am}E}$$

$$t_2 > \frac{p_{max}D + \sqrt{p_{max}D^2(p_{max} + 48\sigma_{am}E)}}{12\sigma_{am}E}$$

$$t_3 > \frac{p_{max}D}{\sigma_{am}E}$$

where: E = 0.7 (joint factor); cs = 1.5 and the material is Stainless steel AISI316.

Once the thicknesses have been found, knowing the length and number of channels and the number of plates, it is possible to evaluate the dimensions of the heat exchanger:

$$H = N_{plates_{tot}}\left(\frac{D}{2} + t_2\right)$$

$$L = 2t_1 + t_3\left(N_{channels\ per\ plate} - 1\right) + N_{channels\ per\ plate}D$$

$$W = L_{channel}\cos(\alpha)\ (\alpha = 0^\circ \text{ for the straight} - \text{channel type})$$

Pressure losses within the exchanger channels are evaluated using Darcy-Weisbach's correlation.

Compact Heat Exchanger (CHX)

A compact heat exchanger of the finned tube type was chosen for the condenser. The condenser cools the CO_2 through the circulation of the external air from environment. The model of this heat exchanger is already present in the EES program libraries [EES, 2020]. The same procedure of the PCHE is then triggered, assuming, for the mechanical design, to utilize the correlations for cylinders under pressure. Therefore knowing the internal diameter and the pressure difference between internal and external, we otbain: $D_{ext} > \frac{D_{int}}{\sqrt{1-\frac{2\Delta p}{\sigma am}}}$; with AISI 316 stainless steel material and safety

coefficient cs = 1.5.

Determined the main dimension of the heat exchanger, the length of the channels $L_{channel}$ is varied and an iterative process runs until UA=$(UA)_{NTU}$.

Data availability

No data was used for the research described in the article.

References

[1] Song J, Ren X, Tian H, Shu G, Gu C, Markides CN. Thermodynamic and economic investigations of transcritical CO2-cycle systems with integrated radial-inflow turbine performance predictions. Appl Therm Eng 2020;165.

[2] Galgaro A, Di Sipio E, Teza G, Destro E, De Carli M, Zarrella A, Emmi G, Manzella A. Empirical modeling of maps of geo-exchange potential for shallow geothermal energy at regional scale. Geothermics 2015;57:173–84.

[3] Bravi M, Basosi R. Environmental impact of electricity from selected geothermal power plants in Italy. J Clean Prod 2014;66:301–8.

[4] Saner D, Juraske R, Kubert M, Blum P, Hellweg S, Bayer P. Is it only CO2 that matters? A life cycle perspective on shallow geothermal systems. Renew Sustain Energy Rev 2010;14:1798–813.

[5] Baldacci A, Mannari M, Sansone F. Greening of geothermal power: an innovative technology for abatement of hydrogen sulphide and mercury emission. In: Proceedings world geothermal congress 2005, antalya, Turkey; 2005. p. 24–9.

[6] Bayer P, Rybach L, Blum PH, Brauchler R. Review of Life Cycle Environmental effects of geothermal power generation. In: Renew.Sustain.Energy rev., vol. 26; 2013. p. 446–63.

[7] Frick S, Kaltschmitt M, Schorder G. A Life cycle assessment of geothermal binary power plants using enhanced low-temperature reservoirs. Energy 2010;35:2281–94.

[8] Basosi R, Bonciani R, Frosali D, Manfrida G, Parisi ML, Sansone F. Life Cycle Analysis of a Geothermal Power Plant: comparison of the environmental performance with other renewable energy systems. Sustainability 2020;12:2786.

[9] Lacirignola M, Blanc I. Environmental analysis of practical design options for enhanced geothermal systems (EGS) through life-cycle assessment. Renew Energy 2013;50:901–14.

[10] Karlsdottir MR, Heinonen J, Palsson H, Palsson OP. Life cycle assessment of a geothermal combined heat and power plant based on high temperature utilization. Geothermics 2020;84.

[11] Parisi ML, Douziech M, Tosti L, Pérez-Lopez P, Mendecka B, Ulgiati S, Fiaschi D, Manfrida G, Blanc I. Definition of LCA guidelines in the geothermal sector to enhance result comparability. Energies 2020;13:3534.

[12] Paulillo A, Cotton L, Raw R, Striolo A, Lettieri P. Geothermal energy in the UK: the life-cycle environmental impacts of electricity production from the United Downs Deep Geothermal Power project. J Clean Prod 2020;249.

[13] Astolfi M, Noto La Diega L, Romano MC, Merlo U, Filippini S, Macchi E. Techno-economic optimization of a geothermal ORC with novel "Emeritus" heat rejection units in hot climates". Renew Energy 2020;147:2810–21.

[14] Fiaschi D, Lifshitz A, Manfrida G, Tempesti D. An innovative ORC power plant layout for heat and power generation from medium to low-temperature geothermal resources. In: Energy conversion and management, vol. 88; 2014. p. 883–93.

[15] Fiaschi D, Manfrida G, Talluri L. Water-ammonia cycles for the utilization of low temperature geothermal resources. In: ASME 2015 power conference; 2015. San Diego, United States.

[16] Fiaschi D, Manfrida G, Rogai E, Talluri L. Exergoeconomic analysis comparison between ORC and Kalina cycles to exploit low and medium-high temperature heat from two different geothermal sites. Energy Convers Manag 2017;154:503–16.

[17] Yari M, Mehr AS, Zare V, Mahmoudi SMS, Rosen MA. Exergoeconomic comparison of TLC (trilateral Rankine cycle), ORC (organic Rankine cycle) and Kalina cycle using a low-grade heat source. In: Energy, vol. 83; 2015. p. 712–22.

[18] Liu Q, Duan Y, Yang Z. Performance analyses of geothermal organic Rankine cycles with selected hydrocarbon working fluids. In: Energy, vol. 63; 2013. p. 123–32.

[19] Liu Q, Duan Y, Yang Z. "Effect of condensation temperature glide on the performance of organic Rankine cycles with zeotropic mixture working fluids. In: Applied energy, vol. 115; 2014. p. 394–404.

[20] Eyerer S, Dawo F, Wieand C, Spliethoff H. Advanced ORC architecture for geothermal combined heat and power generation. Energy 2020;205.

[21] Prananto LA, Zaini IN, Mahendranata BI, Juangsa FB, Aziz M, Soelaiman TAF. Use of Kalina cycle as a bottoming cycle in a geothermal power plant: case studynof the Wayang Windu geothermal power plant. Appl Therm Eng 2018;132:686–96.

[22] Liu X, Wei M, Yang L, Wang X. Thermo-economic analysis and optimization selection of ORC system configurations for low temperature binary-cycle geothermal plant. Appl Therm Eng 2017;125:153–64.

[23] Nami H, Nemati A, Fard FJ. Conventional and advanced exergy analyses of a geothermal driven dual fluid organic Rankine cycle (ORC). Appl Therm Eng 2017;122:59–70.

[24] Karimi S, Mansouri S. A comparative profitability study of geothermal electricity production in developed and developing countries: exergoeconomic analysis and optimization of different ORC configurations. Renew Energy 2018;115:600–19.

[25] Imran M, Usman M, Park BS, Kim HJ, Lee DH. Multi-objective optimization of evaporatator of organic Rankine cycle (ORC) for low temperature geothermal heat source. Appl Therm Eng 2015;80:1–9.

[26] Wu C, Wang SS, Li J. Parametric study on the effects of a recuperator on the design and off-design performances for a CO2 transcritical power cycle for low temperature geothermal plants. Appl Therm Eng 2018;137:644–58.

[27] Schifflechner C, Dawo F, Eyerer S, Wieland C, Spliethoff H. Thermodynamic comparison of direct supercritical CO2 and indirect brine-ORCconcepts for geothermal combined heat and power generation. Renew Energy 2020;161:1292–302. ISSN 0960-1481, https://doi.org/10.1016/j.renene.2020.07.044.

[28] Chasapis D, Misirlis D, Papadopoulos PA, Kleidis K. Thermodynamic analysis on the performance of a low-enthalpy geothermal fields using a CO_2 supercritical binary cycle. Chemical Engineering Transactions 2019;76.

[29] Yin H, Sabau AS, Conklin JC, McFarlane J, Qualls AL. Mixtures of SF6-CO2 as working fluids for geothermal power plants. Appl Energy 2013;106:243–53.

[30] Qiu Y, Li MJ, He YL, Tao WQ. Thermal performance analysis of a parabolic trough solar collector using supercritical CO_2 as heat transfer fluid under non-uniform solar flux. Appl Therm Eng 2017;115:1255–65.

[31] Li H, Zhang Y, Yang Y, Han W, Yao M, Bai W, Zhang L. Preliminary design assessment of supercritical CO2 cycle for commercial scale coal-fired power plants. Appl Therm Eng 2019;158.

[32] Ayub A, Invernizzi CM, Di Marcoberardino G, Iora p, Manzolini G. Carbon dioxide mixtures as working fluid for high-temperature heat recovery: a thermodynamic comparison with transcritical organic Rankine cycles. Energies 2020;13:4014.

[33] Lecompte S, Ntavou E, Tchanche B, Kosmadakis G, Pillai A, Manolakos D, De Paepe M. Review of experimental research on supercritical and transcritical thermodynamic cycles designed for heat recovery application. Appl Sci 2019;9:2571.

[34] Wu Chuang, Wang Shun-sen, Jiang Xihang, Li Jun. Thermodynamic analysis and performance optimization of transcritical power cycles using CO2-based binary zeotropic mixtures as working fluids for geothermal power plants. Appl Therm Eng 2017;115:292–304.

[35] Habibollahzade A, Petersen KJ, Aliahmadi M, Fakhari I, Brinkerhoff JR. Comparative thermoeconomic analysis of geothermal energy recovery via super/transcritical CO2 and subcritical organic Rankine cycles. Energy Convers Manag 2022;251:115008.

[36] Ruiz-Casanova E, Rubio-Maya C, Pacheco-Ibarra JJ, Ambriz-Díaz VM, Romero CE, Wang X. Thermodynamic analysis and optimization of supercritical carbon dioxide Brayton cycles for use with low-grade geothermal heat sources. Energy Convers Manag 2020;216:112978.

[37] Ruiz-Casanova Eduardo, Rubio-Maya Carlos, Pacheco-Ibarra J Jesús, Ambriz-Díaz Víctor M, Torres Pacheco CJ. Edgar Pastor-Martínez, A techno-economic assessment of sCO2 Brayton cycles for low-grade geothermal reservoirs. Geothermics 2023;113:102775.

[38] Manda U, Peles Y, Putnam S. Comparison of heat transfer characteristics of flow of supercritical carbon dioxide and water inside a square microchannel. In: 2021 20th IEEE intersociety conference on thermal and thermomechanical phenomena in electronic systems (iTherm); 2021. p. 1207–13. https://doi.org/10.1109/ITherm51669.2021.9503192. San Diego, CA, USA.

[39] Manda U, Mazumdar S, Peles Y. Effects of cross-sectional shape on flow and heat transfer of the laminar flow of supercritical carbon dioxide inside horizontal microchannels. Int J Therm Sci 2024;201:108992. https://doi.org/10.1016/j.ijthermalsci.2024.108992.

[40] Ellis PF. Downwell pump reliability: geothermal experience update: final report. United States: N. Web 1988. https://doi.org/10.2172/5531454.

[41] Ravier Guillaume, Graff Jean-Jacques, Villadangos Guerric. Operating a lineshaft production pump in a small pump chamber under highly aggressive geothermal fluid conditions: results from the Soultz EGS site. In: Proceedings, World geothermal Congress, Melbourne; 2015.

[42] Aydin H, Akin S, Tüzen MK, Şentürk E. Artificial lifting in liquid dominated high-temperature geothermal fields in Turkey: Lessons learned. In: 46th Workshop on geothermal reservoir Engineering. Stanford, California, USA: Stanford University; 2021, February. p. 15–7.

[43] Nogara James, Zarrouk Sadiq J. Corrosion in geothermal environment: Part 1: fluids and their impact. Renew Sustain Energy Rev 2018;82:1333–46.

[44] Ellis II, Conover MF. Materials selection guidelines for geothermal energy utilization systems (No. DOE/RA/27026-1). Austin, TX: Radian Corp.; 1981 (US).

[45] Duchi V, Minissale AA, Prati F. Chemical composition of thermal springs, cold springs, streams, and gas vents in the Mt. Amiata geothermal region (Tuscany, Italy). J Volcanol Geoth Res 1987;31(3–4):321–32.

[46] Baticci F, Genter A, Huttenloch P, Zorn R. Corrosion and scaling detection in the Soultz EGS power plant, upper rhine graben, France. In: World geothermal Congress, WGC2010. Indonesia: Bali; 2010, April.

[47] Kagel A, Bates D, Gawell K. A guide to geothermal energy and the environment. Washington, DC, USA: Geothermal Energy Association; 2005. Available online: https://www.osti.gov/servlets/purl/897425-q5NDer/. OSTI ID:897425.

[48] Niknam P, Talluri L, Fiaschi D, Manfrida G. Gas purification process in a geothermal power plant with total reinjection designed for the Larderello area. Geothermics 2020;88.

[49] Peralta O, Castro T, Durón M, Salcido A, Celada-Murillo A-T, Márquez C, Navarro-González R, García J, de la Rosa J, Torres R. H_2S emissions from Cerro Prieto geothermal power plant, Mexico, and air pollutants measurements in the area. Geothermics 2013;46:55–65.

[50] Barelli A, Ceccarelli A, Dini I, Fiordelisi A, Giorgi N, Lovari F, Romagnoli P. A review of the Mt. Amiata geothermal system (Italy). In: Proceedings of the World geothermal Congress. Indonesia: Bali; April 2010. p. 25–9.
[51] Di Pippo R. Geothermal power plants—Principles, applications, case studies and environmental impact. third ed. Oxford, UK: Elsevier; 2012.
[52] Zarrouk SJ, Purnanto MH. Geothermal steam-water separators: design overview. Geothermics 2015;53:236–54.
[53] Bruscoli L, Fiaschi D, Manfrida G, Tempesti D. Improving the environmental sustainability of flash geothermal power plants—a case study. Sustainability 2015; 7:15262–83. https://doi.org/10.3390/su71115262.
[54] Szargut J, Morris DR, Steward FR. Exergy analysis of thermal, chemical, and metallurgical processes. Hemisphere Publishing Corporation; 1988.
[55] Kotas TJ. The exergy method of thermal plant analysis. Butterworths; 1985.
[56] Bejan A, Tsatsaronis G, Moran M. Thermal design and optimization. New York, USA: John Wiley & Sons, Inc.; 1996.
[57] Lazzaretto A, Tsatsaronis G. SPECO: a systematic and general methodology for calculating efficiencies and costs in thermal systems. Energy 2006;31:1257–89.
[58] Turton R, Bailie R, Whiting W, Shaeiwitz J. Analysis, synthesis and design of chemical processes. Prentice Hall PTR; 2003.
[59] Schuster A, Karellas S, Kakaras E, Spliethoff H. Energetic and economic investigation of organic rankine cycle applications. In: Applied thermal Engineering; 2009. p. 1809–17.
[60] Chu WX, Li XH, Ma T, Chen YT, Wang QW. Experimental investigation on SCO_2-water heat transfer characteristics in a printed circuit heat exchanger with straight channels. Int J Heat Mass Tran 2017;113:184–94.
[61] Jiang Y, Liese E, Zitney SE, Bhattacharyya D. Design and dynamic modeling of printed circuit heat exchangers for supercritical carbon dioxide Brayton power cycles. Appl Energy 2018;231:1019–32.
[62] Manda Uday, Peles Yoav. A comparative analysis of ammonia and supercritical Carbon Dioxide for microchannel cooling. March 18, 2024.
[63] Le Pierres R, Southall D, Osborne S. Impact of mechanical design issues on printed circuit heat exchangers. In: Proceedings of SCO2 Power cycle symposium; 2011.
[64] Uday Manda, Yoav Peles. Performance Evaluation Criteria of a Star-Shaped Cross-Sectional Microchannel with Supercritical Carbon Dioxide. 2024. Available at SSRN: https://ssrn.com/abstract=4792854. or, https://doi.org/10.2139/ssrn.4792854.
[65] Engineering Equation Solver, EES, F-Chart software. Po box 444042, Madison, WI 53744. www.fchart.com.
[66] Chemical Engineering. Economic Indicators. https://www.chemengonline.com/site/plant-cost-index/.
[67] IRENA. Renewable power generation costs. https://www.irena.org/Publications/2024/Sep/Renewable-Power-Generation-Costs-in-2023; 2023.